MODELING GEOLOGIC STORAGE OF CARBON DIOXIDE: COMPARISON OF NON-HYSTERETIC AND HYSTERETIC CHARACTERISTIC CURVES

Christine Doughty

Lawrence Berkeley National Laboratory

#1 Cyclotron Rd, MS 90-1116

Berkeley, California, 94720, USA

e-mail: cadoughty@lbl.gov

telephone: 1-510-486-6453

fax: 1-510-486-4159

ABSTRACT

Numerical models of geologic storage of carbon dioxide (CO_2) in brine-bearing formations use characteristic curves to represent the interactions of non-wetting-phase CO_2 and wetting-phase brine. When a problem includes both injection of CO_2 (a drainage process) and its subsequent post-injection evolution (a combination of drainage and wetting), hysteretic characteristic curves are required to correctly capture the behavior of the CO_2 plume. In the hysteretic formulation, capillary pressure and relative permeability depend not only on the current grid-block saturation, but also on the history of the saturation in the grid block. For a problem that involves only drainage or only wetting, a non-hysteretic formulation, in which capillary pressure and relative permeability depend only on the current value of the grid-block saturation, is adequate. For the hysteretic formulation to be robust computationally, care must be taken to ensure the differentiability of the characteristic curves both within and beyond the turning-point saturations where transitions between branches of the curves occur. Two example problems involving geologic CO_2 storage are simulated with TOUGH2, a multiphase, multicomponent code for flow and transport code through geological media. Both non-hysteretic and hysteretic formulations are used, to illustrate the applicability and limitations of non-hysteretic methods. The first application considers leakage of CO_2 from the storage formation to the ground surface, while the second examines the role of heterogeneity within the storage formation.

Keywords: Geologic carbon storage, two-phase flow, characteristic curves, hysteresis

INTRODUCTION

Numerical modeling has been used extensively in the past few years to study geologic storage of CO_2 in brine-saturated formations. At depths commonly considered for CO_2 storage (>800 m), CO_2 primarily exists as a gas-like supercritical phase, which is the non-wetting phase, while some CO_2 dissolves in the brine, which is the wetting phase. Interactions between the two fluid phases are represented at the grid-block scale by characteristic curves, that is, capillary pressure and relative permeability functions. The simplest characteristic curves are non-hysteretic – the capillary pressure and relative permeabilities depend only on the local saturation at the current time. A more sophisticated approach is a hysteretic formulation, in which capillary pressure and relative permeabilities depend not only on the current value of the local saturation, but on the history of the local saturation and the process that is occurring: drainage (replacement of wetting phase with non-wetting phase) or wetting (replacement of non-wetting phase with wetting phase, also known as imbibition).

The use of hysteretic characteristic curves is not so critical for the simulation of CO_2 injection periods when the plume is continuously growing (top of Figure 1), because all locations follow the primary drainage branch of the capillary pressure curve at all times, and this branch can be replicated using a non-hysteretic formulation. However, for post-injection periods (bottom of Figure 1), when the CO_2 plume moves upward and updip due to buoyancy forces, different locations experience drainage and wetting at different times, necessitating the use of a hysteretic formulation.

In the sections below, we outline the mathematical formulation of the hysteretic characteristic curves used for modeling CO_2 storage, then briefly describe some of the key numerical issues involved in implementing hysteretic functions into the numerical simulator TOUGH2. Two example problems are presented to illustrate the effects of hysteretic characteristic curves, followed by some concluding remarks.

HYSTERETIC CHARACTERISTIC CURVES

Together, capillary pressure P_c and relative permeabilities k_{rl} and k_{rg} are known as characteristic curves; they control the way the liquid (wetting) phase and gas (non-wetting) phases interact. In a non-hysteretic model, the characteristic curves are single-valued functions of the current grid-block saturation (Figure 2). Different grid blocks may use different characteristic curves, depending on their rock (material) type, but within a given grid block the same characteristic curves are used for all times. In contrast, in a hysteretic model, P_c, k_{rl}, and k_{rg} depend not only on the saturation of the grid block, but also on the history of the saturation of the grid block (Figure 3). Some parameters within the characteristic curve functions depend only on the process (drainage or imbibition) that is occurring, so it is convenient to subdivide the characteristic curves into drainage branches and wetting branches. Other parameters depend on the value of the saturation when the grid block makes a transition from drainage to imbibition or vice versa, the so-called turning-point saturations. Because turning-point saturations differ among all grid blocks, these parameters do as well. The most critical parameter in the latter category is the residual gas saturation, denoted S_{gr}^{Δ}, which is the saturation below which gas is immobile (i.e., the saturation below which immiscible CO_2 is trapped). Under drainage conditions, $S_{gr}^{\Delta} = 0$, but for imbibition, S_{gr}^{Δ} increases as the turning-point saturation between the

drainage curve and wetting curve, denoted S_l^Δ, decreases (Figure 4). Thus, grid blocks that once contained the most CO_2 are those which trap the most CO_2. The maximum possible value of S_{gr}^Δ is $S_{gr\max,}$ which is obtained for the minimum possible value of S_l^Δ, which is generally equal to the irreducible liquid saturation S_{lr}.

Suppose we begin with a brine-saturated formation ($S_l = 1$) and inject immiscible CO_2. As CO_2 reaches each grid block, multiphase flow begins using a capillary pressure curve known as the primary drainage curve (bold red curve in Figure 3). Whenever liquid saturation begins to increase in a given grid block (at S_l^Δ), a transition is made to the first-order scanning wetting curve (thin blue curve in Figure 3), which is interpolated between the primary drainage curve and the primary wetting curve (bold blue curve in Figure 3), using the value of S_l^Δ. If liquid saturation begins to decrease again (not shown in Figure 3), a transition is made to a second-order scanning drainage curve, again obtained by interpolation, which is followed until either (a) liquid saturation drops below its previous minimum value, S_l^Δ, at which point the primary drainage curve is again followed, or (b) liquid saturation again increases, at which point a transition is made to a higher-order scanning wetting curve. Figure 5 illustrates some typical hysteretic capillary pressure paths that include repeated transitions from drainage to wetting and back. All together, four branches of capillary pressure curves are defined: the primary drainage and wetting curves, the first-order wetting scanning curve, the second-order scanning drainage curve, and the third-order scanning wetting curve.

The primary drainage and primary wetting curves are based on the van Genuchten [1] capillary pressure function

$$P_c = -\frac{1}{\alpha^\gamma}\left[\left(\frac{S_l - S_{l\min}}{1 - S_{gr}^{\Delta} - S_{l\min}}\right)^{-\left(\frac{n^\gamma}{n^\gamma - 1}\right)} - 1\right]^{(1/n^\gamma)}, \qquad (1)$$

where γ denotes the branch (*d* for drainage, *w* for wetting) of the capillary pressure curve and α, $S_{l\min}$, and *n* are fitting parameters. For drainage curves, S_{gr}^{Δ}=0. For wetting curves, S_{gr}^{Δ} is given by a modified version of the well-known Land [2] equation as

$$S_{gr}^{\Delta} = \frac{(1 - S_l^{\Delta})}{1 + [1/S_{gr\max} - 1/(1 - S_{lr})](1 - S_l^{\Delta})}. \qquad (2)$$

The parameter $S_{gr\max}$ varies inversely with porosity ϕ and is generally taken as a constant material property. A typical correlation taken from the petroleum literature is given by (M. Holtz, personal communication, 2002; Holtz [3])

$$S_{gr\max} = -0.3136 * \ln(\phi) - 0.1334. \qquad (3)$$

Note from Equation (2) and Figure 4 that when $S_l^{\Delta} = S_{lr}$ (complete drainage of the medium before wetting begins), $S_{gr}^{\Delta} = S_{gr\max}$ and that when $S_l^{\Delta} \sim 1$ (only slight drainage before wetting begins), $S_{gr}^{\Delta} \sim 0$.

Details of the interpolation procedure used to determine the scanning drainage and wetting curves are not reproduced here. Interpolation is based on the dependent domain theory of Mualem [4], implementation of which into TOUGH2 is fully described in Niemi and Bodvarsson [5] and Finsterle et al. [6].

The relative permeability functions also include hysteretic effects arising from the trapped component of the gas phase that develops during wetting. These functions are taken from Parker and Lenhard [7] and Lenhard and Parker [8], who adapted them from the non-hysteretic expressions of van Genuchten [1]. As implemented in TOUGH2, the relative permeability functions are

$$k_{rl}=\sqrt{\bar{S}_l}\left[1-\left(1-\frac{\bar{S}_{gt}}{1-\bar{S}_l^{\Delta}}\right)(1-(\bar{S}_l+\bar{S}_{gt})^{1/m})^m-\left(\frac{\bar{S}_{gt}}{1-\bar{S}_l^{\Delta}}\right)(1-(\bar{S}_l^{\Delta})^{1/m})^m\right]^2 \tag{4}$$

$$k_{rg}=(1-\bar{S}_l-\bar{S}_{gt})^{1/3}(1-(\bar{S}_l+\bar{S}_{gt})^{1/m})^m, \tag{5}$$

where $\bar{S}_l$ and $\bar{S}_l^{\Delta}$ are effective values of liquid saturation S_l and turning-point liquid saturation S_l^{Δ}, respectively, normalized with respect to irreducible liquid-phase saturation S_{lr}:

$$\bar{S}_l=\frac{S_l-S_{lr}}{1-S_{lr}} \tag{6}$$

$$\bar{S}_l^{\Delta}=\frac{S_l^{\Delta}-S_{lr}}{1-S_{lr}}. \tag{7}$$

The parameter $\bar{S}_{gt}$ is the effective value of the trapped gas-phase saturation, which is given by

$$\bar{S}_{gt}=\frac{S_{gr}^{\Delta}(S_l-S_l^{\Delta})}{(1-S_{lr})(1-S_l^{\Delta}-S_{gr}^{\Delta})}. \tag{8}$$

Note that $\bar{S}_{gt}$ is directly proportional to S_{gr}^{Δ}, thus it becomes zero for drainage, greatly simplifying the relative permeability expressions.

NUMERICAL MODEL DEVELOPMENT

TOUGH2 [9] is a general-purpose numerical simulator for multiphase, multicomponent flow in porous and fractured media. It uses a multiphase extension of Darcy's law that includes relative permeability and capillary-pressure effects and incorporates accurate phase-partitioning and thermophysical properties of all fluid phases and components.

The present studies utilize an equation of state package called ECO2 [10], designed to treat a two-phase (liquid, gas), three-component (water, salt, CO_2) system in pressure/temperature regimes above the critical point of CO_2 (P = 73.8 bars, $T = 31^oC$). ECO2 is adapted from EWASG [11], which treats the same components under sub-critical conditions, and is designed for geothermal reservoir simulation. Properties of supercritical CO_2 are calculated from a computer program kindly provided to us by V. Malkovsky (private communication, 1999), that implements the correlations developed by Altunin [12] on the basis of extensive laboratory investigations. Detailed comparison studies with experimental data and with more recent equation of state formulations have shown Altunin's correlations to be very accurate, typically agreeing to within 1% or better with experimental data and with alternative correlations [13].

The simulations presented here emphasize advective processes. Slower flow processes such as aqueous-phase diffusion of dissolved species and the buoyancy effect of dissolved CO_2 are not included. Salt may precipitate out of the brine, but the rock matrix itself is inert. Thus, chemical reactions between CO_2 and rock minerals that could potentially contribute to mineral trapping of CO_2 are not considered.

The precursor of TOUGH2, TOUGH [14] was originally developed with non-hysteretic characteristic curves. The hysteretic capillary pressure functions shown above were implemented in TOUGH in the late 1980's by Niemi and Bodvarsson [5] and hysteretic relative permeability functions were added to TOUGH2 about ten years later by Finsterle et al. [6]. However, the hysteretic model was not numerically efficient enough to be used for 2D or 3D CO_2 storage problems. One crucial modification that we made is to ensure that capillary pressure and relative permeability functions are continuous and differentiable within and beyond the turning-point saturations that bound the different branches of the curves. Extension beyond the turning-point saturations is needed for two reasons. First, when saturation is incremented during the Newton-Raphson iteration used by TOUGH2 to solve the non-linear governing equations, it may cross a turning-point saturation. Second, there is a threshold value of saturation change below which no branch transitions are made, which can enable saturation to cross a turning-point saturation. Additionally, coding was added to handle an element drying out ($S_l < S_{lr}$) and then rewetting. Finally, an option has been added to delay branch transitions to the end of the time step. This has the effect of making the fully implicit time-stepping normally employed by TOUGH2 partially explicit. With these modifications, simulations using the hysteretic formulation are computationally competitive with those using a non-hysteretic formulation.

Several features of the implementation of Equations (1) through (8) in TOUGH2 that were originally hardwired in the code are now provided as user options. For example, S_{gr}^{Δ} is always zero for the primary drainage branch of the capillary pressure curve and always given by Equation (2) for all wetting branches, but it now may be defined either way for the second-order scanning drainage curve, according to the user's conceptual model of

non-wetting phase trapping. Furthermore, a different definition may be used for the capillary pressure curve than is used for the relative permeability curves.

APPLICATIONS

Two problems related to CO_2 storage are simulated using both hysteretic and non-hysteretic formulations for characteristic curves. The first problem considers leakage of CO_2 from the storage formation to the ground surface, while the second examines the role of heterogeneity within the storage formation.

Leakage from Formation to Surface

The model for the leakage study is shown in Figure 6. CO_2 is injected into a porous formation 100 m thick located at a depth of 1000 m. The porosity of the formation is 25%, horizontal permeability is 200 md, and vertical permeability is 100 md. The lower boundary of the porous formation is the base of the model, which is a closed boundary. Above the porous formation is an overburden, which extends to the surface. A range of properties has been considered for the overburden by Doughty and Myer [15], to study the fate of leaking CO_2 plumes, but here we just consider an overburden with the same properties as the storage formation itself.

Initially, the brine saturation is 100% everywhere in the model, pore pressure is hydrostatic with a pressure of 1 bar at the surface, and temperature follows the geothermal gradient of 30^oC/km, with the temperature at the surface and base of the model held constant at 15^oC and 48^oC, respectively. The salinity of the pore water is assumed to be 100,000 ppm.

Thermodynamic conditions represented in ECO2 include super- and sub-critical CO_2, but for sub-critical conditions, ECO2 does not distinguish between liquid and gaseous CO_2, and associated phase changes cannot be represented. Thus for sub-critical conditions encountered between the storage formation and the ground surface (typically at depths less than 700 m), ECO2 can only model flow paths that do not cross the saturation line. This can be accomplished by choosing a relatively warm surface temperature to keep the geothermal gradient on the gas side of the saturation line, and considering slow enough flows so that the CO_2 plume remains in near thermodynamic equilibrium with its surroundings, and thus remains close to the geothermal gradient (Figure 7). A more detailed discussion of this issue may be found in Doughty and Myer [15].

The numerical simulations were carried out using a 2D axisymmetric model composed of 61 layers each containing 41 grid blocks. All grid blocks are 20 m thick except for a few layers near the surface, which are thinner to better resolve surface arrival time. Radial grid block extent is 20 m out to a distance of 600 m, after which it steadily increases to produce an infinite-acting model.

The numerical simulations begin with injection of 900,000 tons of CO_2 into the porous formation at a constant rate of 30,000 tons per day for 30 days. This quantity of CO_2 corresponds roughly to the emissions of a 1,000 MW coal fired power plant for 30 days. After injection stops, the only driving force in the model tending to cause movement of the CO_2 is buoyancy. Simulations continue for 1,000 years.

Tables 1 and 2 summarize the parameters of the hysteretic and non-hysteretic characteristic curves, respectively. The non-hysteretic models use van Genuchten [1] liquid relative

permeability and capillary pressure functions, and a Corey [16] gas relative permeability function. The first case has a small residual gas saturation ($S_{gr} = 0.01$), which is believed to be appropriate for CO_2 injection periods (drainage), and creates a "slippery" CO_2 plume that moves easily through the formation with little trapping. The second case has a large residual gas saturation ($S_{gr} = 0.25$), which is believed to be appropriate for the trailing edge of the CO_2 plume during the post-injection period (wetting), and produces a "sticky" CO_2 plume that traps substantial amounts of CO_2 as it moves.

Figure 8 shows snapshots of the free-phase CO_2 plumes at a series of times during the 1,000-year simulation period for the two non-hysteretic cases. Below depths of 700 m, the CO_2 is supercritical whereas above 700 m the CO_2 is gaseous. The fate of the CO_2 is very different for the two cases: much of the slippery plume has reached the surface within 10 years and nearly all the CO_2 has escaped within 100 years, whereas the sticky plume never reaches the surface and remains entirely trapped indefinitely.

Figure 9 shows the CO_2 plume development for the hysteretic model. During the one-month injection period, the slippery non-hysteretic model and hysteretic model give similar results. Thereafter, neither non-hysteretic model fully captures the dynamics of plume evolution. The hysteretic model enables the leading edge of the plume, where drainage occurs and S_{gr} is small, to continue to advance, while the trailing edge of the plume, where imbibition occurs and S_{gr} is large, to remain largely trapped.

Figure 10 shows the capillary pressure and relative permeability paths followed for several locations in the CO_2 plume using the hysteretic model. All paths begin at $S_l = 1$ along the primary drainage curve; the transition to a wetting scanning curve occurs at S_l^{Δ} (shown by

arrows); as $|P_c| \rightarrow 0$ on the wetting curves, $S_l \rightarrow (1 - S_{gr}^{\Delta})$ (shown by black dots), with S_{gr}^{Δ} given by Equation (2). Thus grid blocks near the plume center, which get much drier during the injection period and therefore have a small S_l^{Δ}, have a much larger S_{gr}^{Δ}, and consequently trap more CO_2, than do grid blocks that the plume barely reaches.

Figure 11 shows snapshots of the variable that identifies which branch of the capillary pressure curve is being followed: the primary drainage curve, the first-order wetting scanning curve, the second-order drainage scanning curve, or the third-order wetting scanning curve. At one month (the end of the injection period), the entire plume is draining. At three months, the upper half of the plume is draining and the lower half is wetting. By one year, most of the plume is wetting, with only a narrow band right at the leading edge draining. Note that as a plume spreads out, gas saturation decreases, which is equivalent to wetting. Thus, even in the absence of movement, a spreading plume will be wetting. At late times, the dominance of higher-order scanning curves indicates that saturation changes are small and tend to be oscillatory, as the bulk of the plume becomes immobile.

Figure 12 shows the time variation of the mass fraction of CO_2 in different forms (mobile, immobile, and dissolved) integrated over the entire model, for all three cases. Mass fraction is calculated by dividing the mass present at each time by the total amount of CO_2 injected. The mobile, immobile, and dissolved fractions sum to the total fraction. The total fraction remains one if the CO_2 plume does not reach the surface. It is clear that neither non-hysteretic model successfully reproduces the behavior shown by the hysteretic model, in which the quantity of immobile CO_2 is low during the injection period, but rapidly increases after injection ceases.

Storage in a Heterogeneous Formation

The second example problem considers CO_2 injection and storage into a heterogeneous formation representing a fluvial-deltaic geology, consisting primarily of high-permeability sands, intercut with low-permeability shales (Figure 13). Porosity ranges from 0.1 to 0.32, and increases with permeability. The 1 km by 1 km by 100 m thick model is created stochastically based on well logs and a simplified conceptualization of the regional depositional setting [17]. It has 30 layers, each containing 400 grid blocks. The top and bottom boundaries are closed, and the lateral boundaries are held at constant pressure. Injection of CO_2 occurs through a single well penetrating the lower half of the formation at a constant rate of 2000 tons per day for a period of 20 years, after which the evolution of the CO_2 distribution is followed for 80 years. The present study uses the same characteristic curves as for the leakage problem described previously (Tables 1 and 2).

Figures 14 and 15 show the evolution of free-phase, supercritical CO_2 for non-hysteretic models for the slippery-plume case (small S_{gr}) and sticky-plume case (large S_{gr}), respectively. It is clear that the choice of S_{gr} has a strong impact on CO_2 behavior, especially during the rest period after injection ends. During the injection period, the sticky plume is more compact than the slippery plume, with somewhat higher values of gas saturation. After injection ends, nearly all of the free-phases CO_2 exits through the lateral boundaries of the model for the slippery plume, whereas substantial amounts remain in place for the sticky plume.

Figure 16 shows the CO_2 plume for the hysteretic model. During the injection period, the hysteretic and non-hysteretic slippery-plume case give similar results, but during the post-

injection rest period neither non-hysteretic model agrees closely with the hysteretic model. Modeled CO_2 saturations are too low for the slippery-plume case and too high for the sticky-plume case. Neither model can reproduce the behavior obtained using hysteretic characteristic curves wherein the leading edge of the plume, where drainage is occurring, is more mobile than is the trailing edge, where imbibition is occurring.

Interestingly, there is one location where CO_2 remains trapped for all three cases, near the top of the model at about x = 200 m, y = 400 m, in a pocket of sand surrounded by low-permeability shale (compare Figures 13, 14, 15, and 16). This suggests that where structural trapping mechanisms exist, CO_2 becomes trapped regardless of multi-phase flow effects, and it is not so important how characteristic curves are defined. Conversely, where structural trapping is absent (or uncertain), properly representing multi-phase flow effects through characteristic curves becomes critical.

Figure 17 shows snapshots of the branches of the capillary pressure curve being followed for the hysteretic model, indicating which parts of the model are draining and wetting at various times. Unlike the leakage problem, here wetting begins before the injection period ends, a consequence of the subtle interplay between fluid flow and geologic heterogeneity. Most of the injection-period wetting occurs in the lower portion of the model, indicating that early in the injection period, flow into this region is greater than at later times. Thus, buoyancy-driven upward flow through gaps in the shale layers must increase with time. Such an increase is expected, as low-viscosity CO_2 replaces high-viscosity brine in the upper portion of the model.

Figure 18 shows the time variation of the mass of CO_2 in different forms (mobile, immobile, and dissolved) integrated over the entire model, for all three cases. A quasi-steady state develops by about 8 years into the injection period, in which CO_2 injection is approximately balanced by flow out the lateral boundaries of the model. Within about 10 years after the end of injection, the system again reaches a quasi-steady state, in which nearly all the CO_2 is immobile or dissolved. Neither non-hysteretic model produces the correct CO_2 masses throughout the entire simulation period. In particular, the non-hysteretic slippery-plume case underpredicts how much immiscible CO_2 can be stored, whereas the non-hysteretic sticky-plume case overpredicts it. Neither non-hysteretic model produces the sharp increase in immobile CO_2 that occurs when injection ends.

CONCLUDING REMARKS

The prevailing conceptual model for two-phase flow involving immiscible CO_2 and brine considers the residual gas saturation to be strongly process-dependent, with a small value during drainage and a potentially large value during imbibition that increases with the maximum historical value of gas saturation. It is therefore necessary to employ hysteretic characteristic curves when modeling a problem that encompasses both drainage and wetting. If only the injection of CO_2 is considered, with a continually growing CO_2 plume, then a non-hysteretic formulation using properties relevant for drainage, in particular a small value of residual gas saturation, should suffice. The same holds true if structural trapping constrains CO_2 plume movement, precluding imbibition. However, for the more general case of injection is followed by a rest period in which the CO_2 plume can move due to regional pressure gradients or buoyancy forces, both drainage (at the leading edge of the CO_2 plume) and imbibition (at the trailing edge of the CO_2 plume) will occur. In this

case, a hysteretic model that incorporates a small value of residual gas saturation during drainage and a potentially large, history-dependent value during imbibition is required to correctly capture the behavior of the CO_2 plume, whose trailing edge is less mobile than its leading edge.

As the applications show, non-hysteretic models do a poor job of reproducing CO_2 plume migration. With a small value of S_{gr}, the injection period can be modeled adequately, but after injection ends far too little CO_2 is immobilized at the trailing edge of the plume (e.g., upper frames in Figure 8). With a large value of S_{gr}, the injected CO_2 plume is too compact, and after injection ends too much CO_2 is trapped because the invasion process still occurring at the plume leading edge is not correctly modeled (e.g., lower frames in Figure 8). Using a process-dependent value of S_{gr} (S_{gr}^{Δ}) in a hysteretic formulation avoids both problems. Although a small amount of CO_2 remains mobile at the leading edge of the plume (e.g., Figure 9 shows that CO_2 reaches the surface after about 100 years), the bulk of the plume is immobile (the integrated mass balance shown in Figure 12 indicates that the amount of CO_2 leaving the subsurface is negligibly small). The variability in plume mobility actually has some additional advantages for sequestration. With a more mobile leading edge and less mobile trailing edge, the CO_2 plume will tend to stretch out, exposing more of the plume to native brine, which enhances dissolution, and to the formation itself, which enhances mineral reactions that take up CO_2.

ACKNOWLEDGMENTS

The careful reviews of Stefan Finsterle and Curt Oldenburg are gratefully appreciated. This work was supported by the ZERT (Zero Emissions Research and Technology) and

GEO-SEQ programs, through the Assistant Secretary for Fossil Energy, Office of Coal and Power Systems through the National Energy Technology Laboratory, and by Lawrence Berkeley National Laboratory under Department of Energy Contract No. DE-AC02-05CH1123.

REFERENCES

[1] van Genuchten MTh. A closed-form equation for predicting the hydraulic conductivity of unsaturated soils. Soil Science Society of America Journal 1980;44(5):892-8.

[2] Land CS. Calculation of imbibition relative permeability for two- and three-phase flow from rock properties. SPE Journal 1969;9:149-56.

[3] Holtz MH. Reservoir characterization applying residual gas saturation modeling, example from the Starfak T1 reservoir, middle Miocene Gulf of Mexico. M.Sc. Thesis. Austin: University of Texas; 2005.

[4] Mualem Y. A modified dependent domain theory of hysteresis. Soil Science 1984;137(5): 283-91.

[5] Niemi A, Bodvarsson GS. Preliminary capillary hysteresis simulations in fractured rocks, Yucca Mountain, Nevada. Journal of Contaminant Hydrology 1988;3:277-91.

[6] Finsterle S, Sonnenborg TO, Faybishenko B. Inverse modeling of a multistep outflow experiment for determining hysteretic hydraulic properties. In Pruess K, editor. Proceedings of the TOUGH workshop ’98, Rep. LBNL-41995, Berkeley: Lawrence Berkeley National Laboratory; 1998, p. 250-6.

[7] Parker JC, Lenhard RJ. A model for hysteretic constitutive relations governing multiphase flow, 1. Saturation-pressure relations. Water Resources Research 1987;23(12):2187-96.

[8] Lenhard RJ, Parker JC. A model for hysteretic constitutive relations governing multiphase flow, 2. Permeability-saturation relations. Water Resources Research 1987;23(12):2197-205.

[9] Pruess K, Oldenburg C, Moridis G. TOUGH2 user's guide, version 2.0. Rep. LBNL-43134. Berkeley: Lawrence Berkeley National Laboratory; 1999.

[10] Pruess K, García J. Multiphase flow dynamics during CO2 disposal into saline aquifers. Environmental Geology 2002;42:282-95.

[11] Battistelli A, Calore C, Pruess K. The simulator TOUGH2/EWASG for modeling geothermal reservoirs with brines and non-condensible gas. Geothermics 1997;26(4):437-64.

[12] Altunin VV. Thermophysical properties of carbon dioxide (in Russian). Moscow: Publishing House of Standards; 1975.

[13] García JE. Fluid dynamics of carbon dioxide disposal into saline aquifers. PhD thesis. Berkeley: University of California; 2003.

[14] Pruess K. TOUGH user's guide. Rep. LBL-20700. Berkeley: Lawrence Berkeley National Laboratory; 1987.

[15] Doughty C, Myer LR. Scoping calculations on leakage of CO2 in geologic storage. In: McPherson B and Sundquist E, editors. Science and technology of carbon sequestration, Washington DC: American Geophysical Union; 2006, in press.

[16] Corey AT. The interrelation between gas and oil relative permeabilities. Producers Monthly 1954;November:38-41.

[17] Doughty C, Pruess K. Modeling supercritical carbon dioxide injection in heterogeneous porous media. Vadose Zone Journal 2004;3(3):837-47.

FIGURE CAPTIONS

Figure 1. Schematic of CO_2 injection period (top), in which drainage occurs at all plume boundaries (orange), and post-injection period (bottom), in which drainage occurs at the leading edge of the plume on the right (orange) and wetting occurs at the trailing edge of the plume on the left (green) as the plume migrates, e.g. by buoyancy forces.

Figure 2. Non-hysteretic characteristic curves. The dots show values of residual saturation for each curve. Typically, drainage is associated with a small or zero value of residual gas saturation (red curves) whereas wetting is associated with a large value (blue curves). Characteristic curves may differ between grid blocks, but each grid block uses the same characteristic curves (and hence the same values of residual saturation) at all times.

Figure 3. Illustration of hysteretic characteristic curves. The red curves show the primary drainage curves, the heavy blue curve is the primary wetting curve, and the thin blue curves show some possible wetting scanning curves. The turning points between drainage and wetting (diamonds) differ among grid blocks, hence so do the wetting curves and residual gas saturations (circles).

Figure 4. Residual gas saturation S_{gr}^{Δ} as a function of turning-point saturation S_l^{Δ}, for S_{lr} = 0.3 and various values of $S_{gr\max}$.

Figure 5. Hysteretic capillary pressure paths for scenario (a) (left frame) and scenario (b) described in text. Each path begins at $S_l = 1$, $P_c = 0$.

Figure 6. Schematic diagram of the first 400 m of the axisymmetric model for the leakage problem.

Figure 7. Typical pressure-temperature conditions encountered by plumes rising from a storage formation at 1000 m depth (pressure about 120 bars) to the ground surface (pressure 1 bar). To avoid crossing the saturation line, a surface temperature of 15°C is specified for the present studies.

Figure 8. CO_2 plume evolution with non-hysteretic models. Top: slippery plume with S_{gr} = 0.01. Bottom: sticky plume with S_{gr} = 0.25. The single black contour line shows $S_g = 0$.

Figure 9. CO_2 plume evolution with hysteretic model. The single black contour line shows $S_g = 0$.

Figure 10. Hysteretic capillary pressure (top) and relative permeability (bottom) paths for several locations within CO_2 plume for the leakage problem.

Figure 11. Branches of capillary pressure curves for hysteretic model.

Figure 12. Mass fractions of CO_2 in various forms for the leakage problem, integrated over the entire model.

Figure 13. Cut-away view of the 3D model used for the heterogeneity problem. Horizontal permeability is shown for each material.

FIGURES

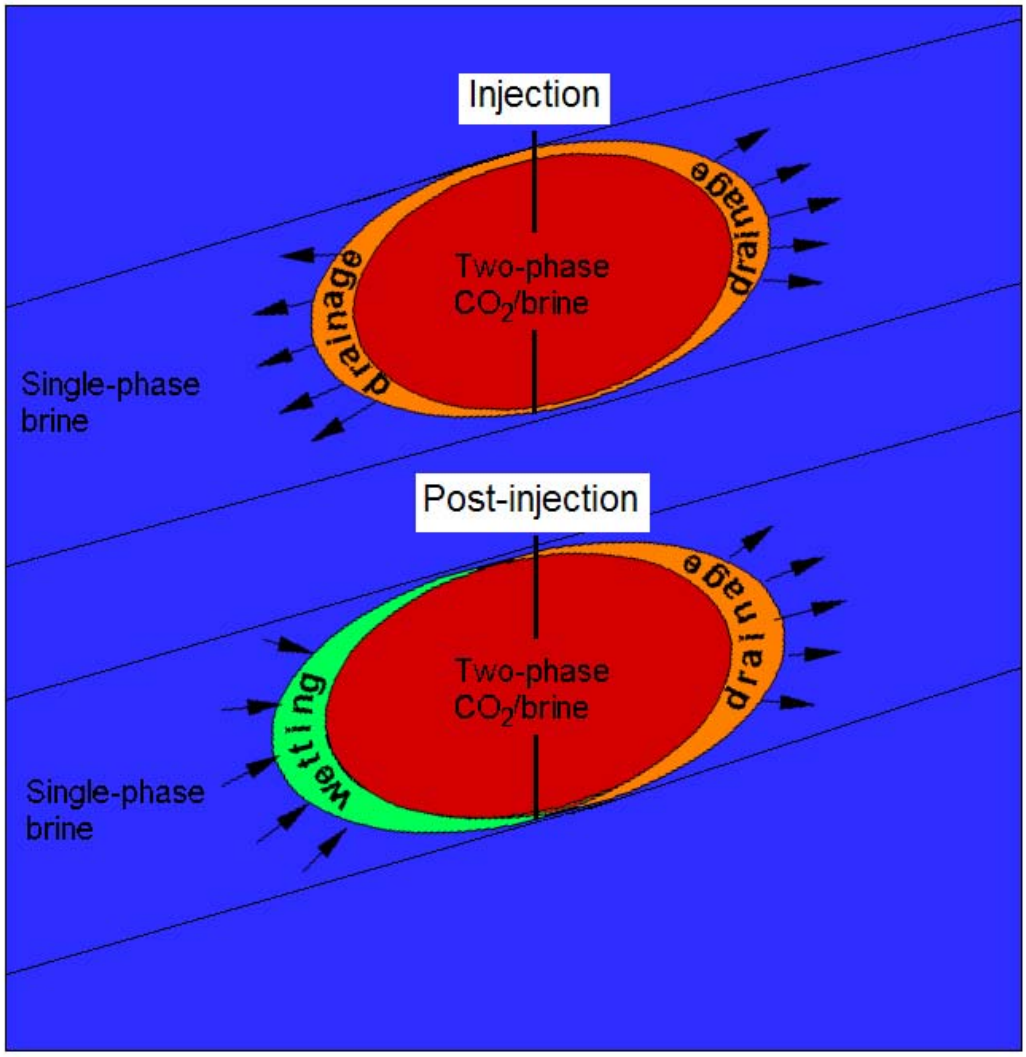

Figure 1. Schematic of CO_2 injection period (top), in which drainage occurs at all plume boundaries (orange), and post-injection period (bottom), in which drainage occurs at the leading edge of the plume on the right (orange) and wetting occurs at the trailing edge of the plume on the left (green) as the plume migrates, e.g. by buoyancy forces.

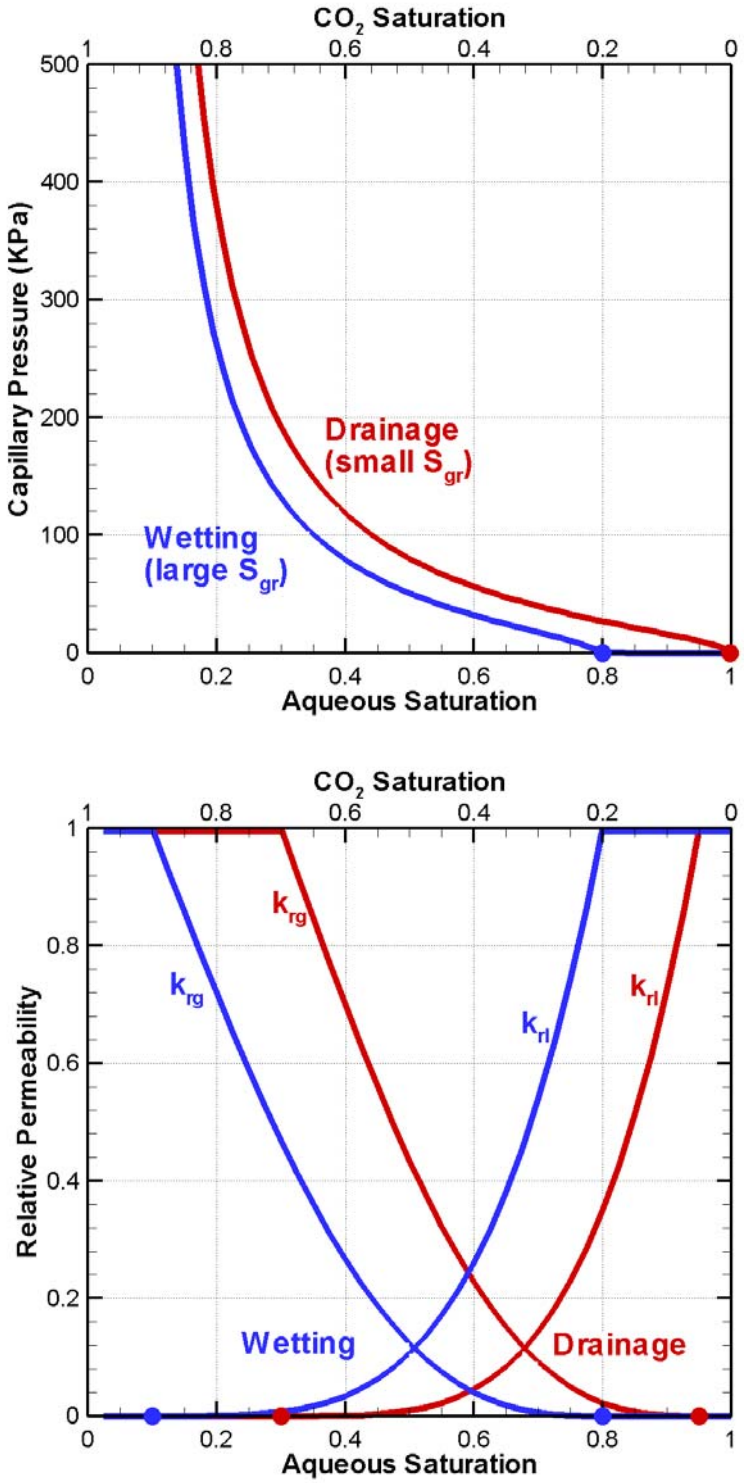

Figure 2. Non-hysteretic characteristic curves. The dots show values of residual saturation for each curve. Typically, drainage is associated with a small or zero value of residual gas saturation (red curves) whereas wetting is associated with a large value (blue curves). Characteristic curves may differ between grid blocks, but each grid block uses the same characteristic curves (and hence the same values of residual saturation) at all times.

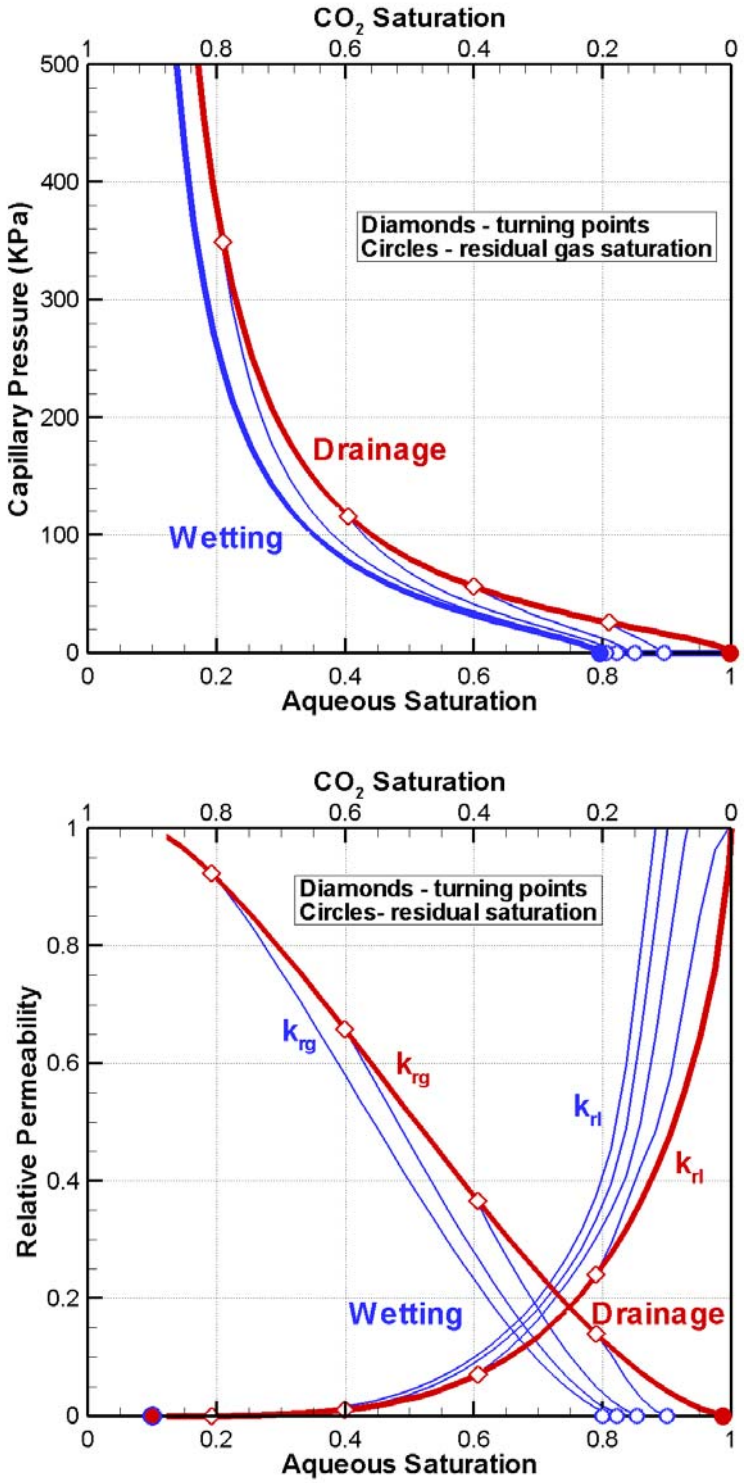

Figure 3. Illustration of hysteretic characteristic curves. The red curves show the primary drainage curves, the heavy blue curve is the primary wetting curve, and the thin blue curves show some possible wetting scanning curves. The turning points between drainage and wetting (diamonds) differ among grid blocks, hence so do the wetting curves and residual gas saturations (circles).

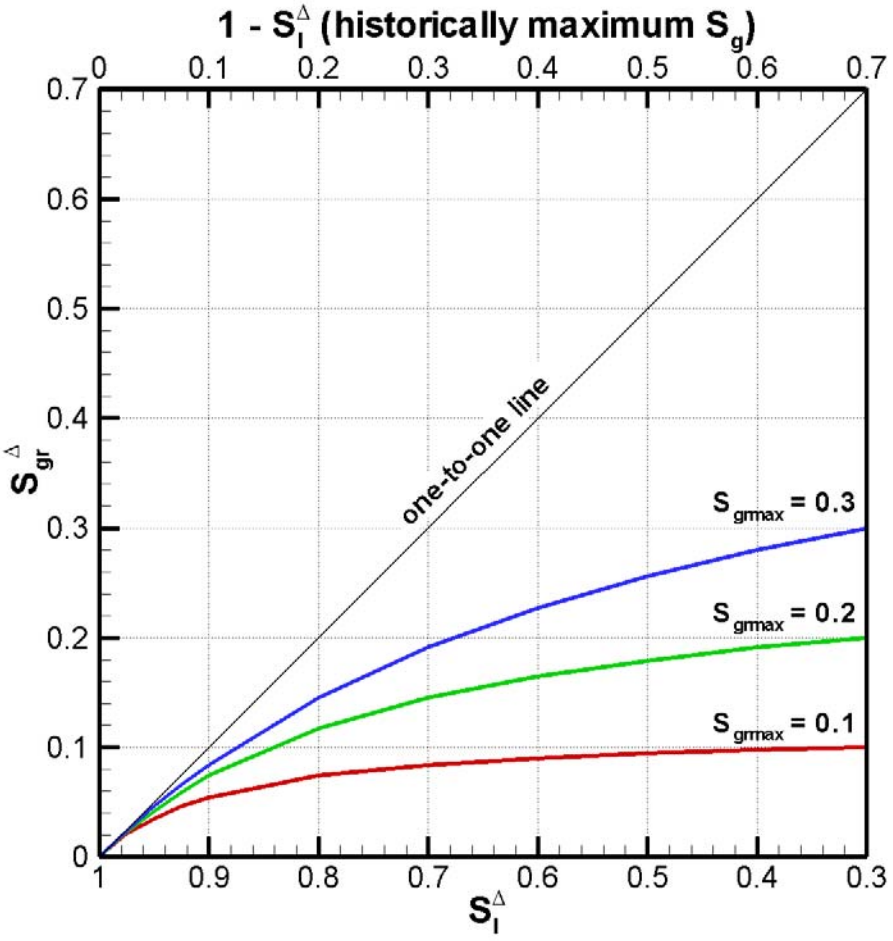

Figure 4. Residual gas saturation S_{gr}^{Δ} as a function of turning-point saturation S_l^{Δ}, for S_{lr} = 0.3 and various values of $S_{gr\max}$.

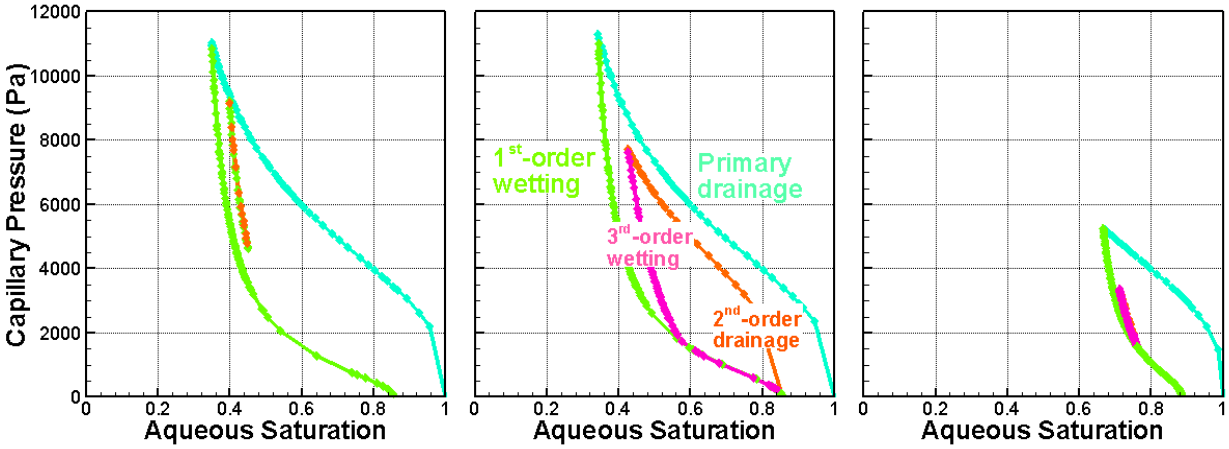

Figure 5. Hysteretic capillary pressure paths for scenario (a) (left frame) and scenario (b) described in text. Each path begins at $S_l = 1$, $P_c = 0$.

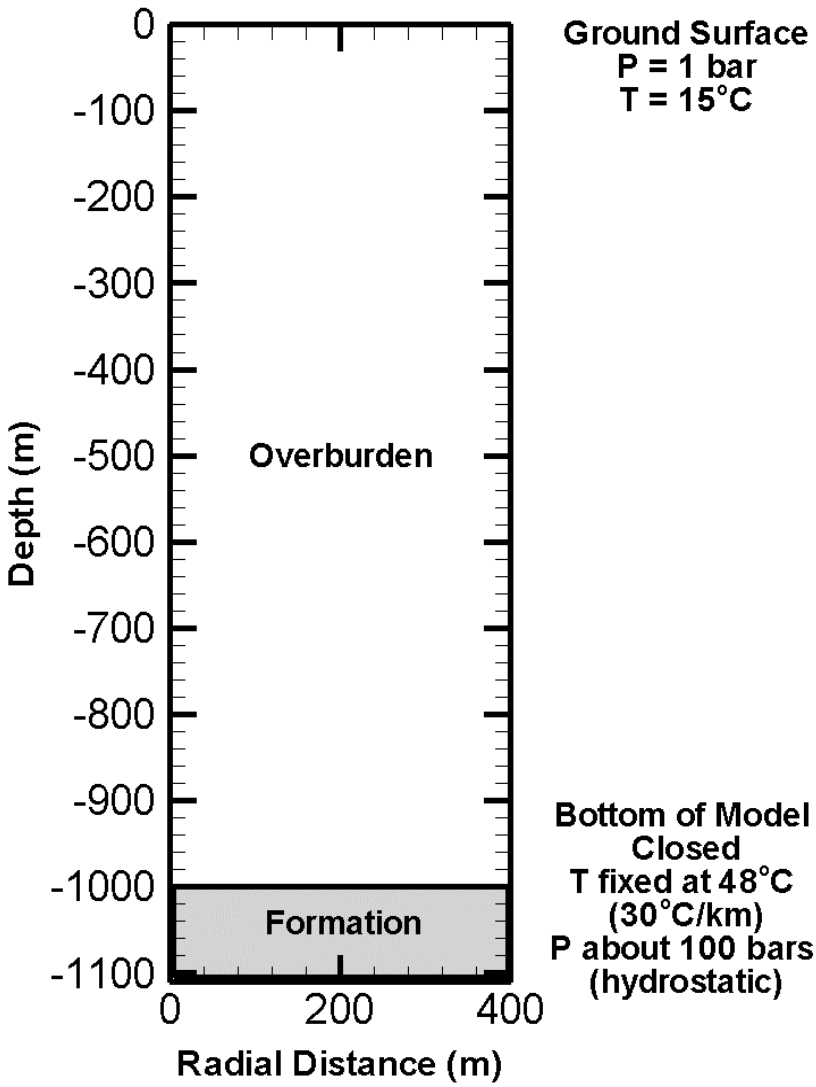

Figure 6. Schematic diagram of the first 400 m of the axisymmetric model for the leakage problem.

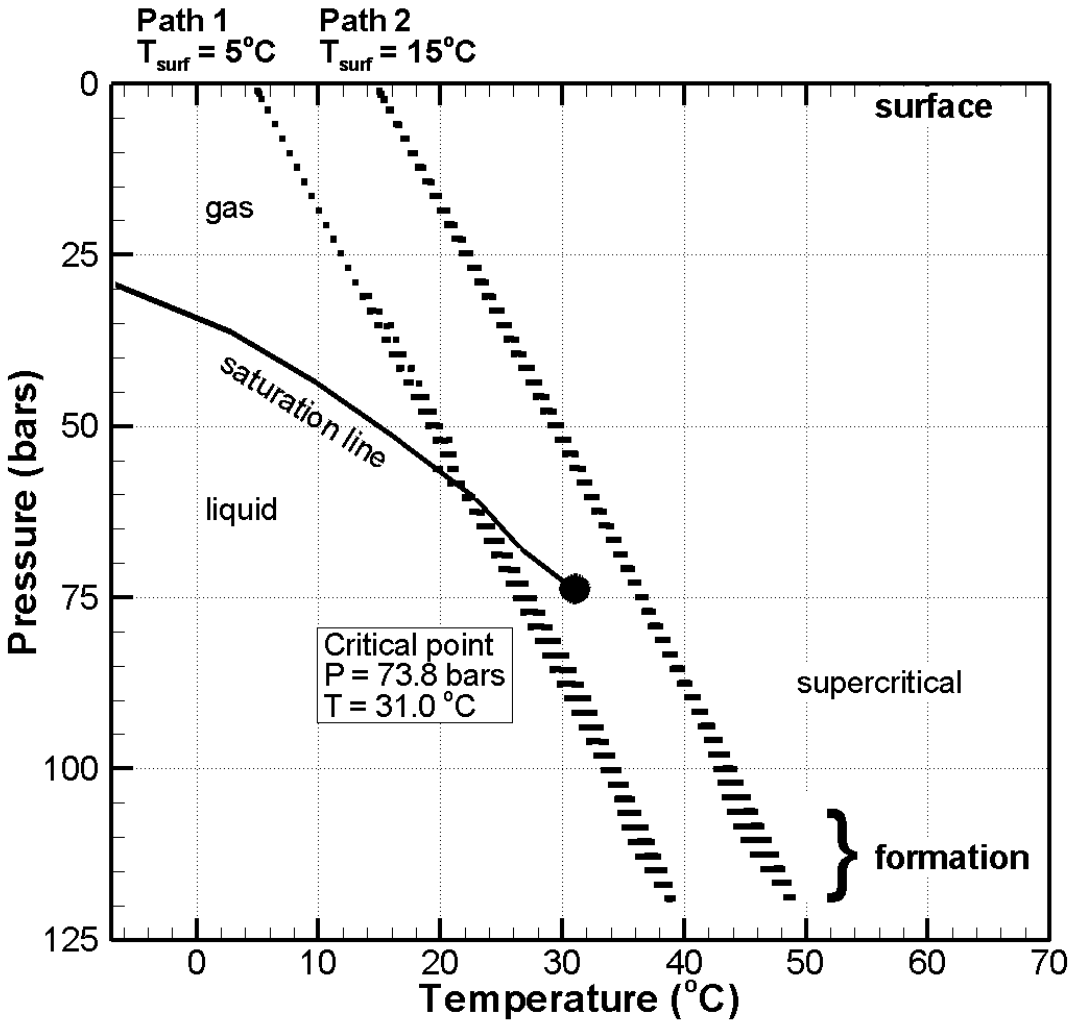

Figure 7. Typical pressure-temperature conditions encountered by plumes rising from a storage formation at 1000 m depth (pressure about 120 bars) to the ground surface (pressure 1 bar). To avoid crossing the saturation line, a surface temperature of 15°C is specified for the present studies.

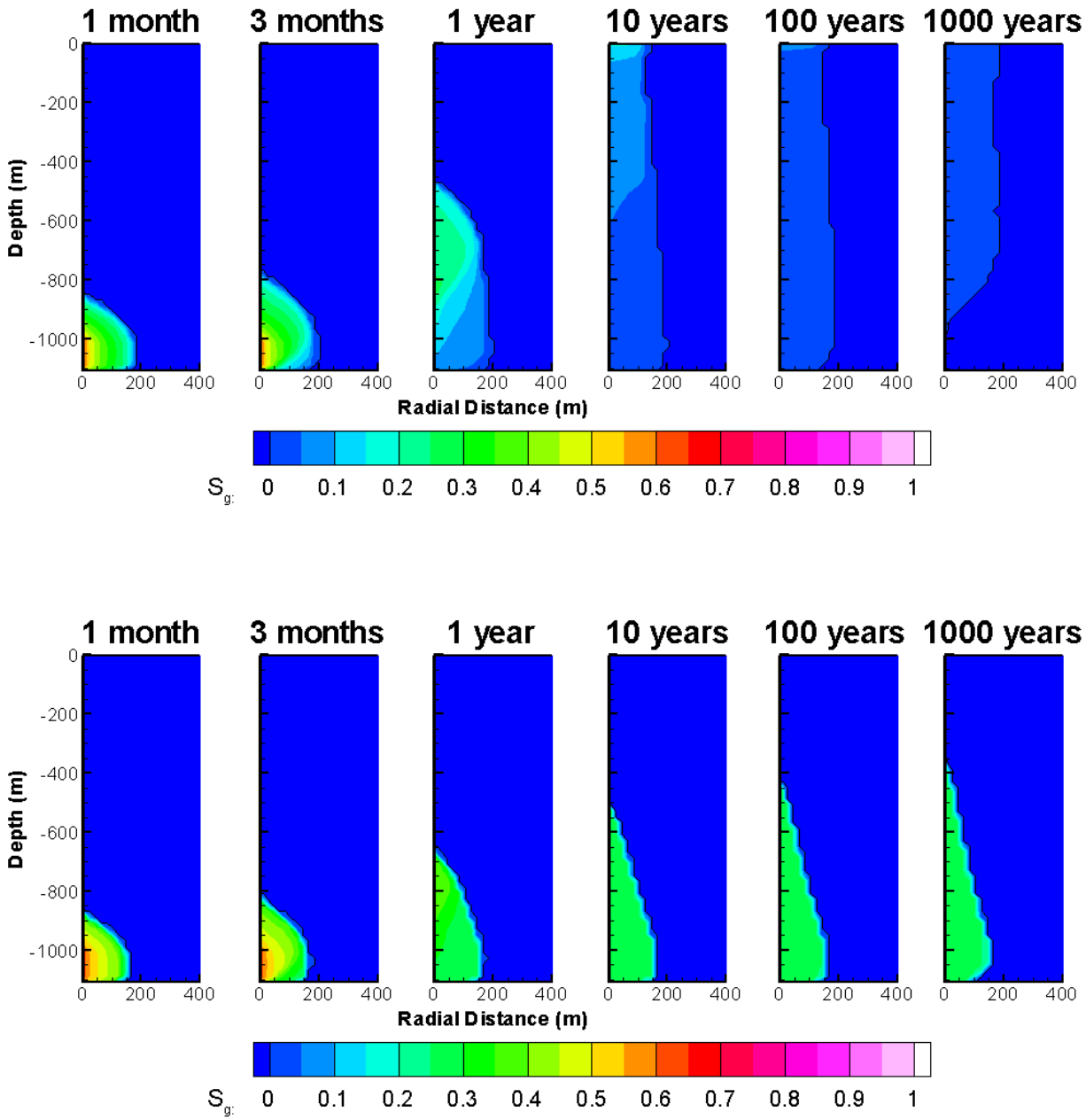

Figure 8. CO_2 plume evolution with non-hysteretic models. Top: slippery plume with S_{gr} = 0.01. Bottom: sticky plume with S_{gr} = 0.25. The single black contour line shows S_g = 0.

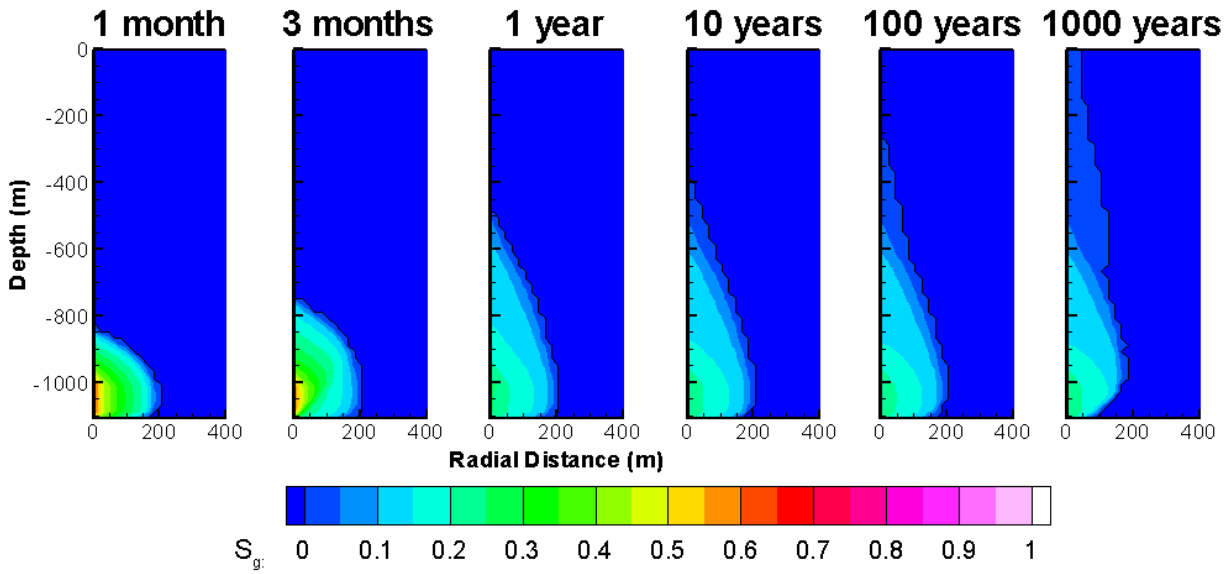

Figure 9. CO_2 plume evolution with hysteretic model. The single black contour line shows $S_g = 0$.

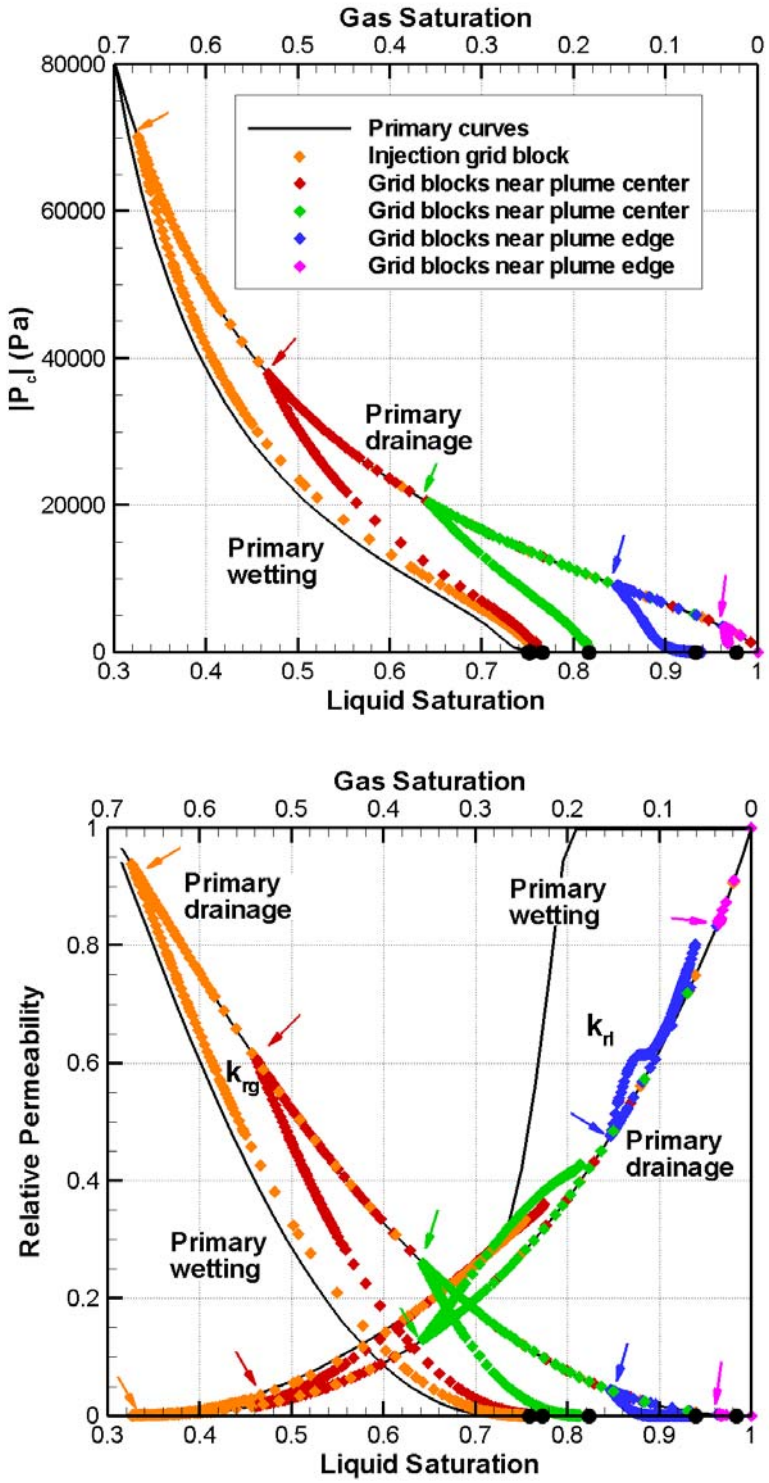

Figure 10. Hysteretic capillary pressure (top) and relative permeability (bottom) paths for several locations within CO_2 plume for the leakage problem.

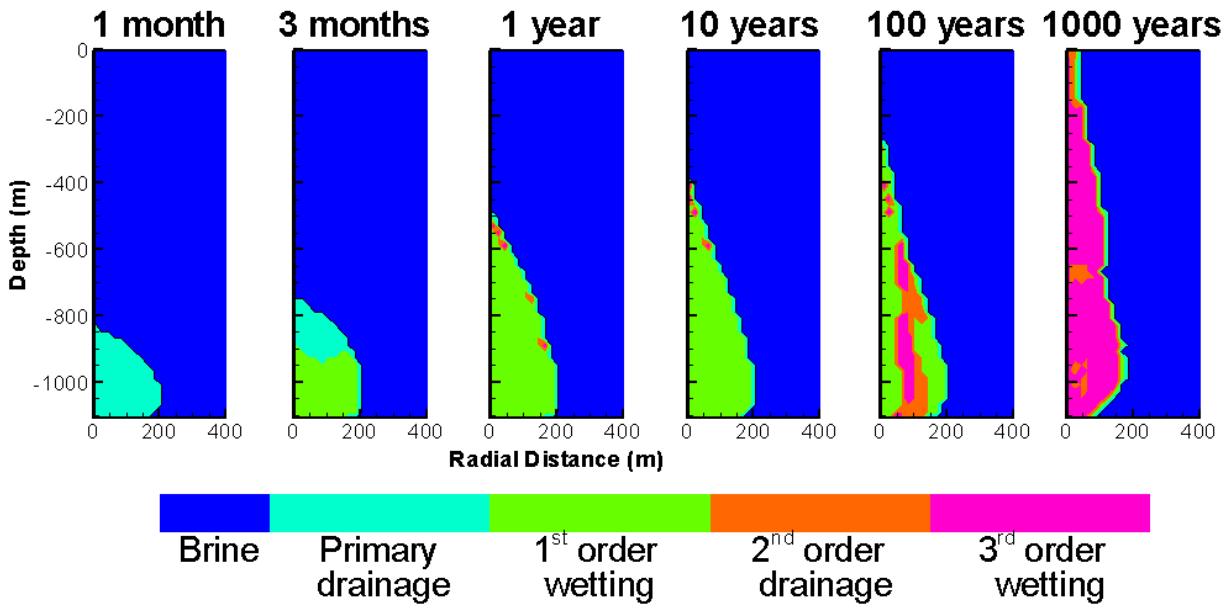

Figure 11. Branches of capillary pressure curves for hysteretic model.

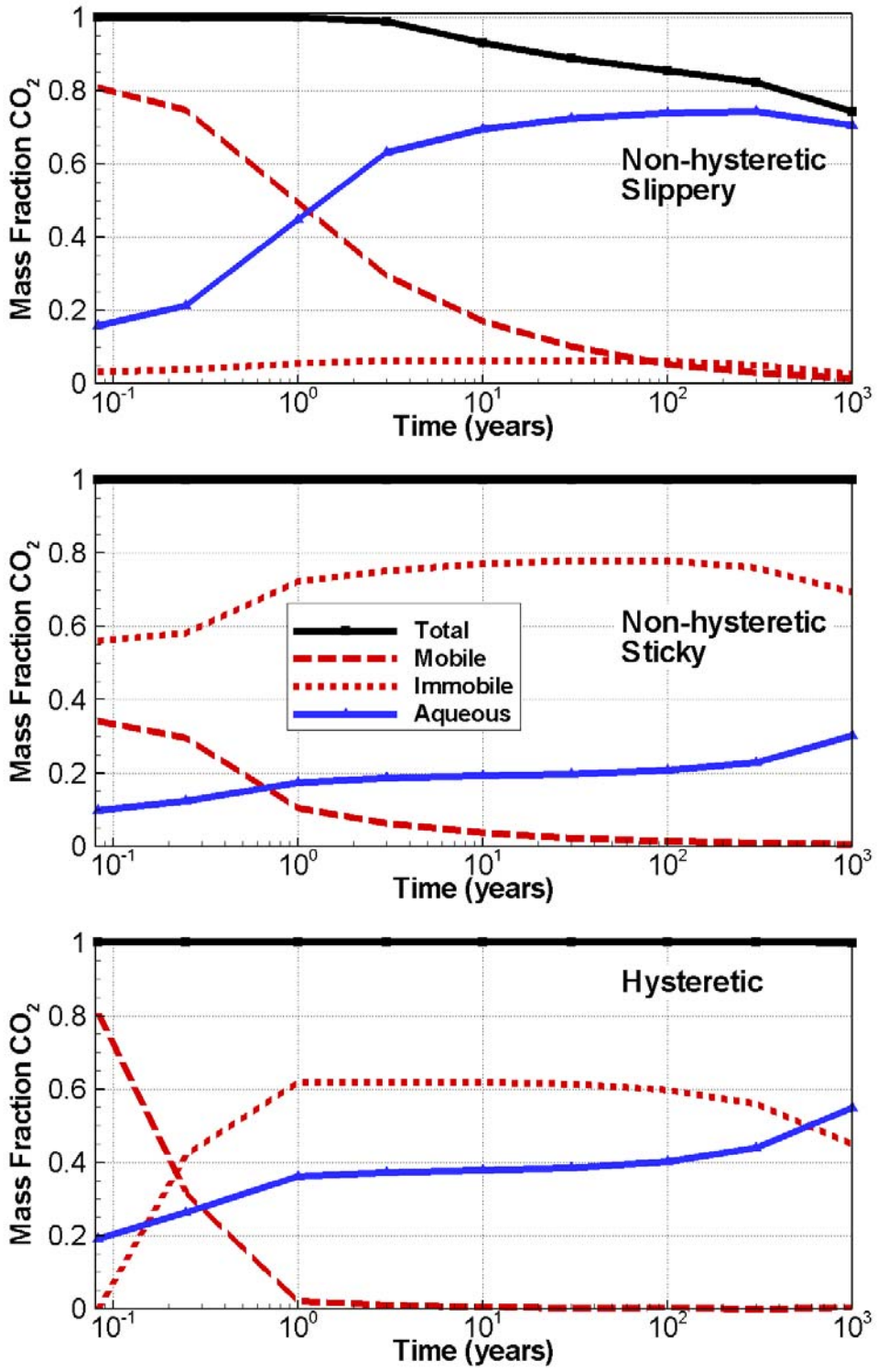

Figure 12. Mass fractions of CO_2 in various forms for the leakage problem, integrated over the entire model.

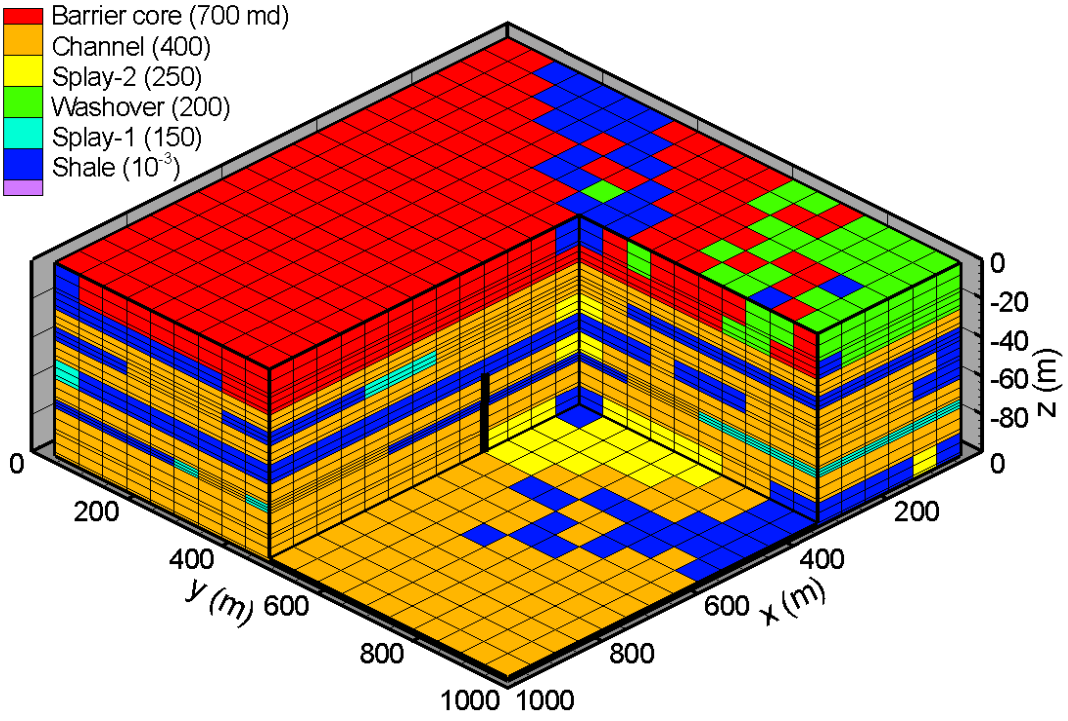

Figure 13. Cut-away view of the 3D model used for the heterogeneity problem. Horizontal permeability is shown for each material.

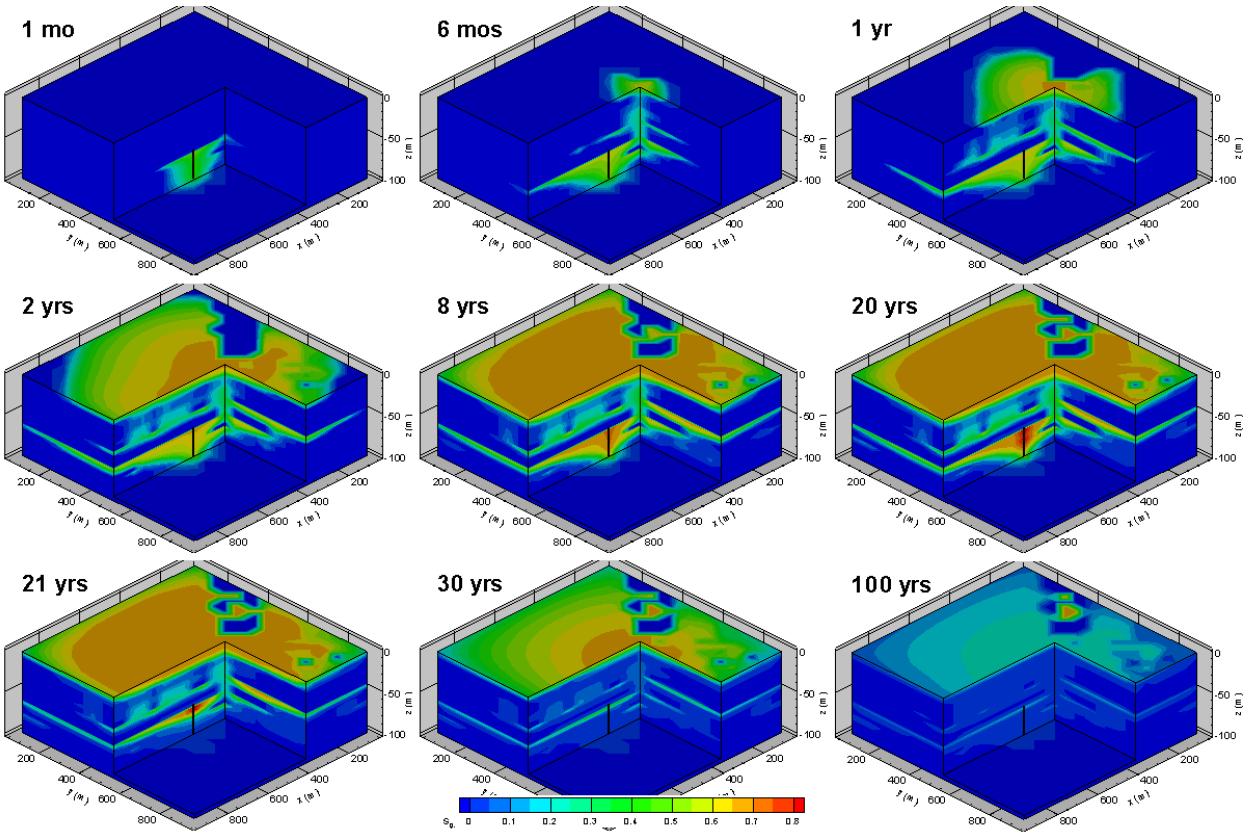

Figure 14. CO_2 plume evolution for non-hysteretic model, slippery-plume case (small S_{gr}).

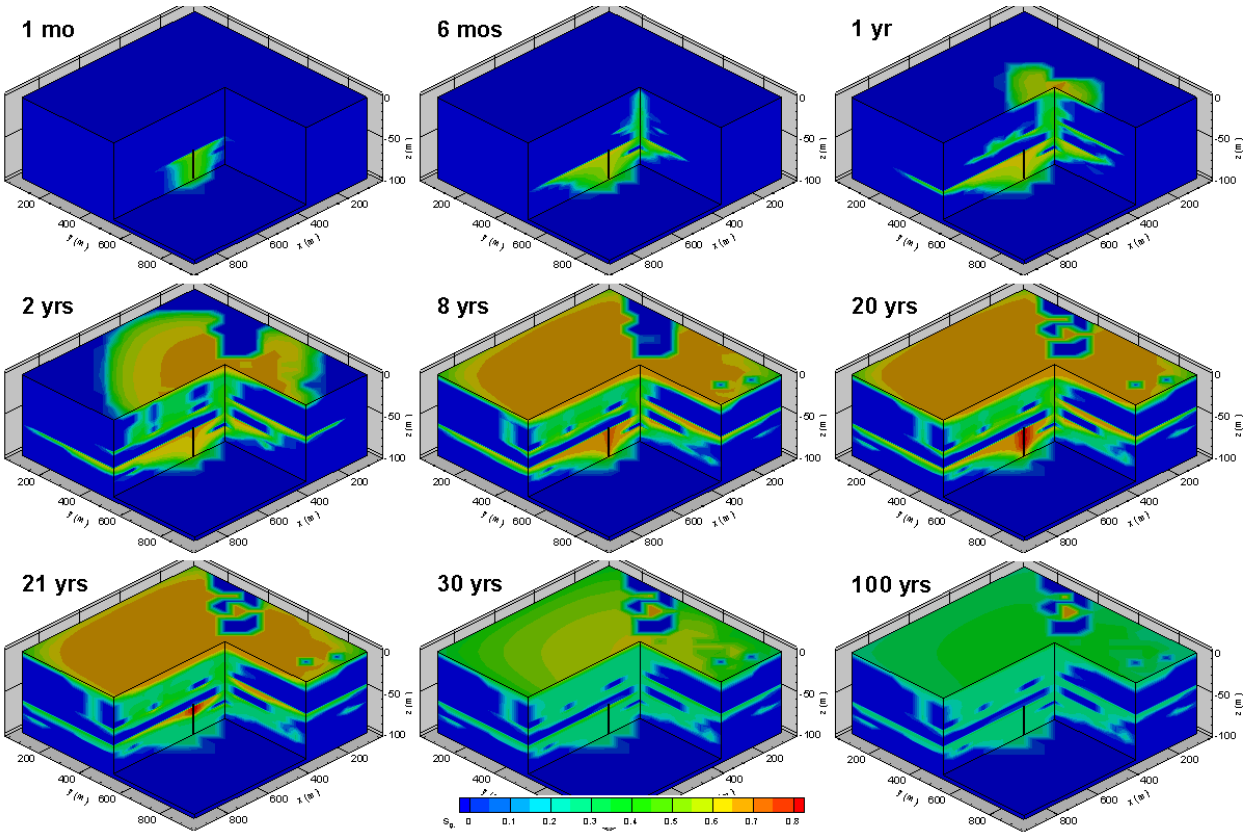

Figure 15. CO_2 plume evolution for non-hysteretic model, sticky-plume case (large S_{gr}).

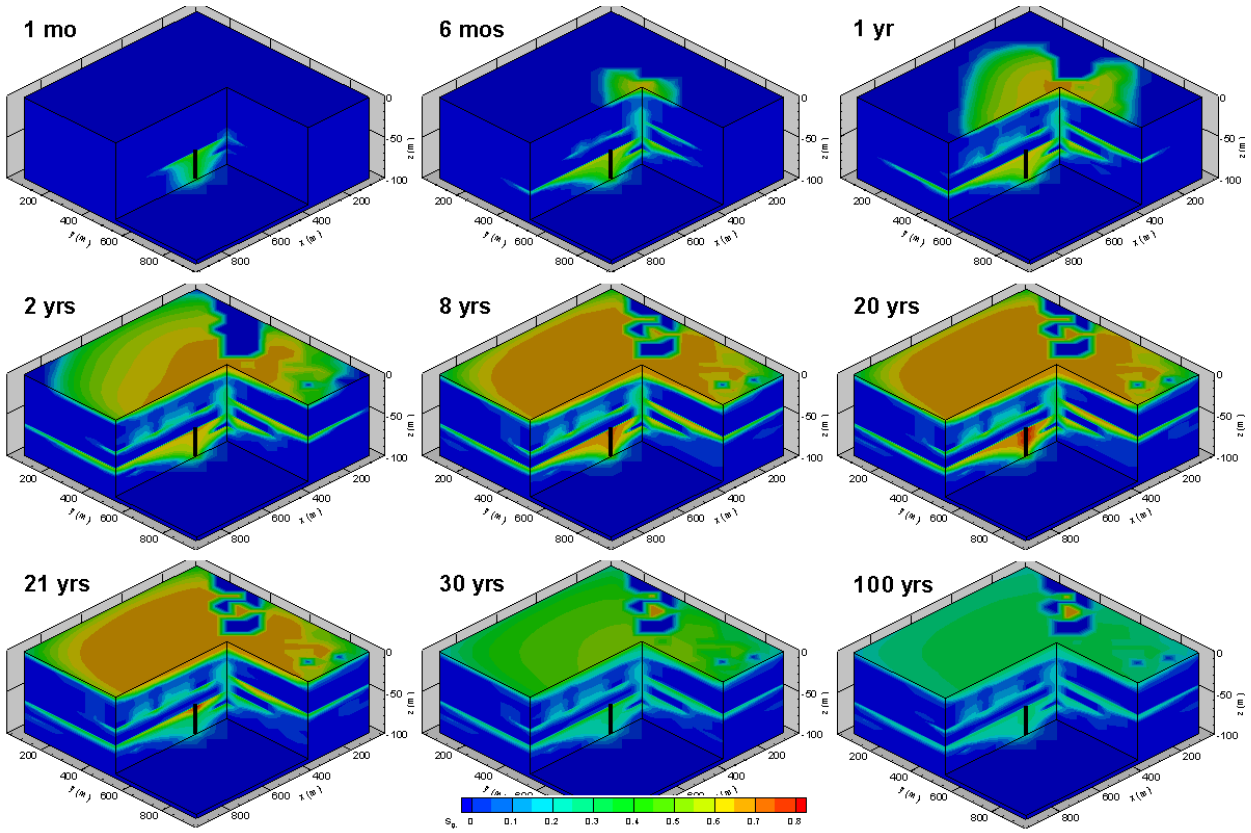

Figure 16. CO_2 plume evolution for hysteretic model.

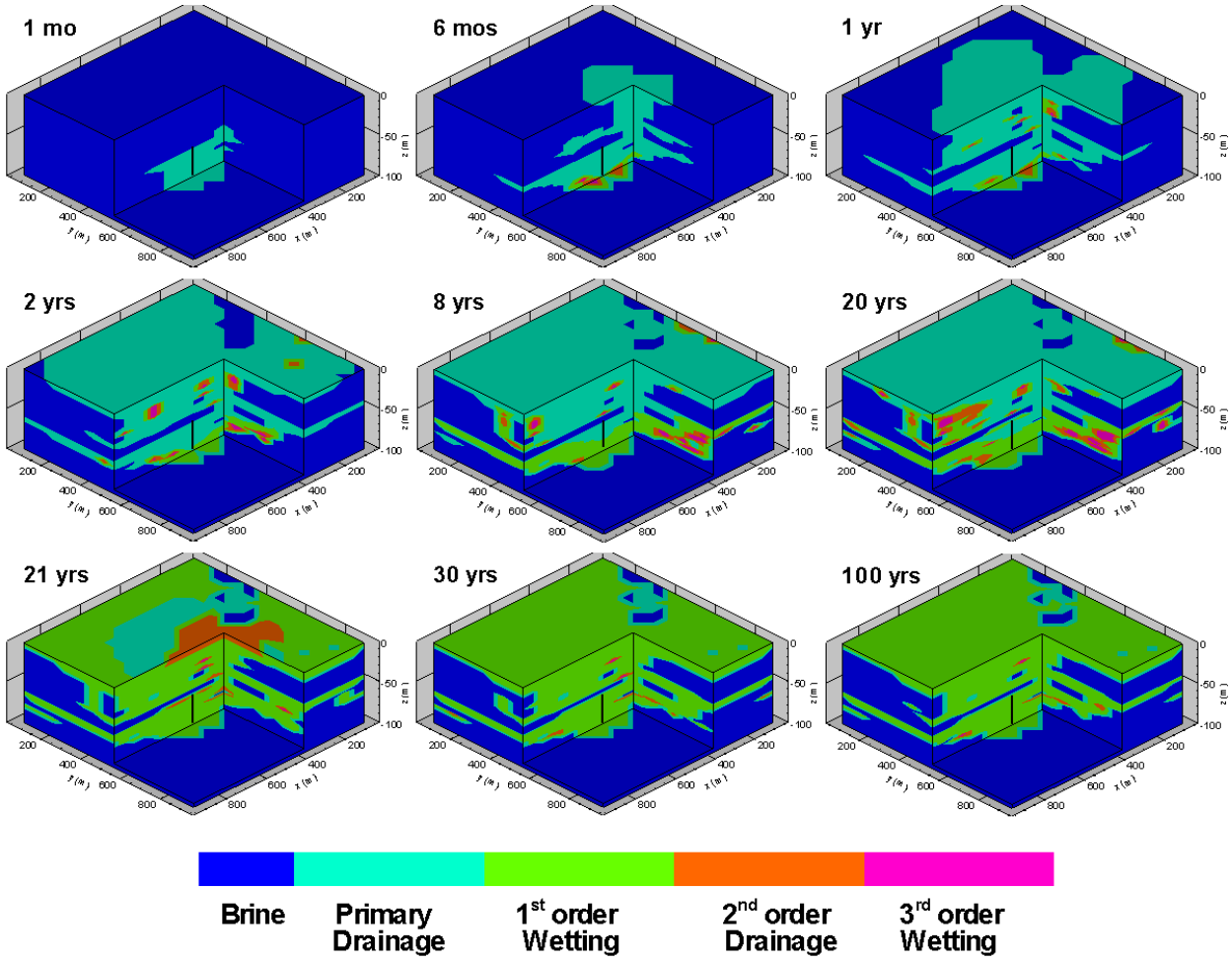

Figure 17. Branches of capillary pressure curves for hysteretic model.

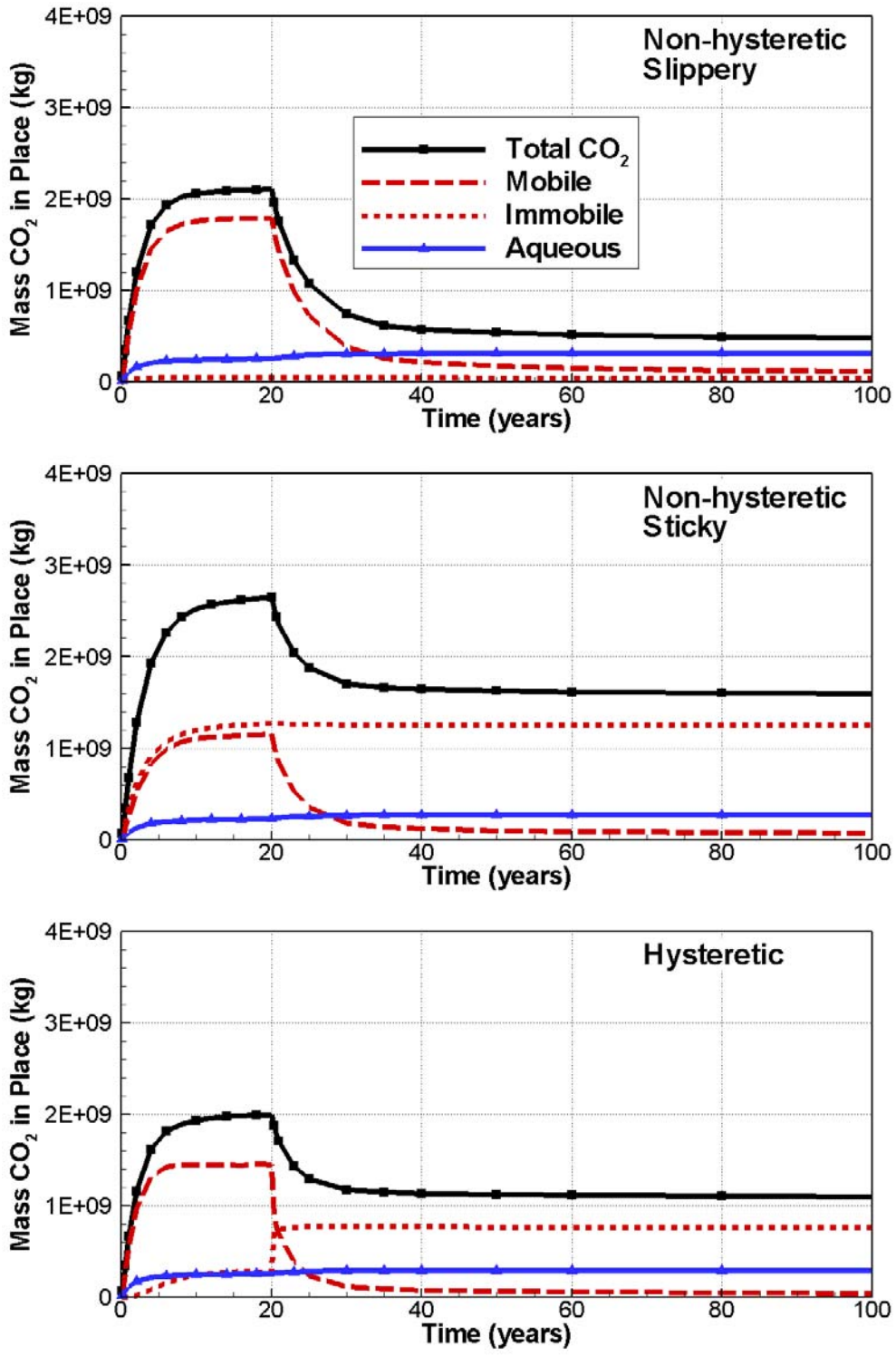

Figure 18. Mass of CO_2 in various forms for the heterogeneity problem, integrated over the entire model.

TABLES

Table 1. Hysteretic characteristic curve parameters.

Parameter	Value
Capillary pressure parameters (Eqs. 1 and 2)	
$1/\alpha^d$ and $1/\alpha^w$ (bars)	0.133
n^d and n^w	1.7
$S_{l\min}$	0.03
$S_{gr\max}$	0.25
Relative permeability parameters (Eqs. 4 and 5)	
m	0.917
S_{lr}	0.3

Table 2. Non-hysteretic characteristic curve parameters. Parameters are chosen to mimic the drainage branch (slippery plume) and wetting branch (sticky plume) of the hysteretic formulation.

Parameter	**Slippery plume**	**Sticky Plume**
Capillary pressure parameters Eq. 1 with S_{gr}^{Δ} replaced by a constant		
$1/\alpha$ (bars)	0.133	0.133
n	1.7	1.7
$S_{l\min}$	0.03	0.03
Constant S_{gr}^{Δ}	0	0.25
Liquid relative permeability parameters Eq. 4 with $\overline{S}_{gt} = 0$ and $\overline{S}_l = (S_l - S_{lr})/(S_{ls} - S_{lr})$		
m	0.917	0.917
S_{lr}	0.3	0.3
S_{ls}	1.0	0.92
Gas relative permeability parameters Corey curve $k_{rg} = (1-S^*)^2 - (1-S^{*2})$, with $S^* = (S_l - S_{lr})/(1 - S_{lr} - S_{gr})$		
S_{lr}	0.3	0.3
S_{gr}	0.01	0.25